IOP Conference Series: Materials Science and Engineering

PAPER • **OPEN ACCESS**

Development and calibration of a structural simulation method of CF-SMC composite parts processed by compression molding

To cite this article: M Delvò *et al* 2021 *IOP Conf. Ser.: Mater. Sci. Eng.* **1038** 012074

View the article online for updates and enhancements.

This content was downloaded from IP address 93.65.121.183 on 12/03/2021 at 07:53

Development and calibration of a structural simulation method of CF-SMC composite parts processed by compression molding

M Delvò[1], G Nicoletto[1] and E Riva[1]

[1]Dipartimento di Ingegneria e Architettura, Università degli Studi di Parma, Italy

enrica.riva@unipr.it

Abstract. The need for the reduction in CO2 production in automotive field increasingly leads manufacturers to consider fiber-reinforced composite materials that are however costly to processes. Discontinuous fiber composite materials, like CF – SMC, are a competitive candidate because they are transformed by the high productivity compression molding technology. On the negative side, their structural complexity introduces high variability in the mechanical performance that needs to be considered at the design stage. This contribution describes the development of a structural modeling strategy for parts made of CF-SMC processed by compression molding. It is based the statistical material model proposed by Feraboli implemented here in a FEA-based structural analysis procedure. After validation and calibration of a specific CF-SMC material, the proposed procedure is applied to the simulation of the structural response of a compression molded part of complex geometry subjected to know loading conditions.

1 Introduction

Increasing fuel prices and strict clean-air environment requirements motivate researchers and automobile manufacturers to identify new CFRP applications for the serial production of structural parts. CFRP applications for established sectors such as aerospace are of relatively large dimensions and simple geometry, while structural components for automobiles are relatively small and their geometries are complex. Furthermore, the high productivity required by the automotive sector has focused the research on out-of-autoclave material forms and automated processes, [1]. Therefore, the main goal of future CFRP applications in automotive is the identification of material and process combination resulting in mechanical performance typical of the long fiber composite combined with high formability and productivity typical of short-fiber reinforced polymers, [2-3].

An increasingly successful process for composite is compression molding (CM), a closed-mold high-volume process where metal dies are mounted in a hydraulic press, [4]. The material charge is placed in the mold which are heated; then the two mold halves are closed, and high pressure is applied. Cycle time ranges from one to 10 minutes depending on part size and thickness. Compression molded parts are characterized by net size and shape, two excellent finished surfaces, and outstanding part-to-part repeatability. Trimming and finishing costs are minimal, [1].

CF-SMC (Carbon Fiber Sheet Molding Compound) are composite materials of this kind, characterized by a relatively high carbon fiber volume fraction and excellent flow-ability are readily compression molded to produce complex parts. Randomly-oriented pre – preg strands (CF-ROS) of relatively long

Content from this work may be used under the terms of the Creative Commons Attribution 3.0 licence. Any further distribution of this work must maintain attribution to the author(s) and the title of the work, journal citation and DOI.
Published under licence by IOP Publishing Ltd

(up to 25 mm) carbon fibers in a thermoplastic matrix have been proposed in [3]. They achieve a significantly higher CF volume fraction (i.e. 53% and more) than usual reinforcements, approaching the 60% fiber volume fraction of conventional CFRP, [6].

Fig. 1. Example of CF-SMC automotive chassis produced by CM, [5].

CF-SMCs are characterized by high delamination resistance, quasi-isotropic in-plane stiffness, high out-of-plane strength and stiffness, and low notch sensitivity, [6-9], and thus they favor the metal-to-CFRP conversion. However, the random nature of the fiber reinforcement within the matrix significantly affects the mechanical response due to complicated load transfer mechanisms, with fiber ends acting as stress concentrating factors that lead to the nucleation of cracks and development of complex damage mechanisms. Experimental tests show that the prediction of mechanical response is limited by the significant scatter in stiffness and strength, [6]. For example, Fig. 2(a) shows a CF-SMC plate produced by CM with standard tensile specimens directed in orthogonal directions and extracted by water jet. Tensile tests of Fig. 2(b) demonstrate considerable variability of the mechanical behavior.

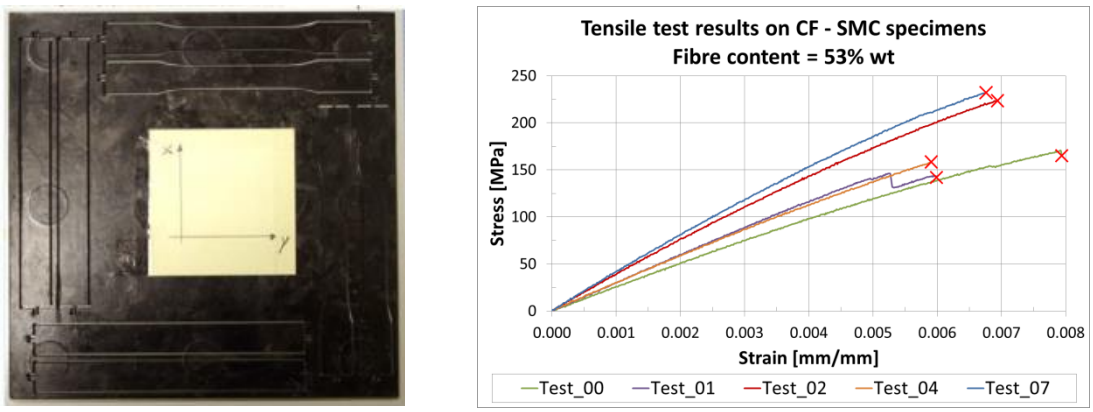

(a) (b)

Fig. 2. (a) Tensile specimens in CF-SMC (53%) plate and (b) typical scatter in tensile response.

The structural complexity of CF-ROS composites and the associated variable mechanical behavior cannot be described and modeled using a deterministic approach, [6]. Specific material models and simulation strategies are required to eliminate expensive and time consuming trial-and-error physical validation and move toward effective part design and virtual validation. This contribution is aimed at this industrial need and is divided into three parts: 1) the statistical material modeling using homogenized properties as proposed by Feraboli, [9], is adopted and implemented into a specific FEA code; 2) the FEA-based statistical model of the CF-SMC behavior is calibrated using original tensile tests; 3) the FEA-based statistical model is applied to the prediction of the mechanical behavior of a real structural component from the automotive sector.

2 Model description and implementation

A presentation of the peculiar nature of the CF-SMC structure after CM processing may clarify the material modeling approach used here, [9]. The material volume extracted from a plate is presented in its original form in Fig. 3(a) and in terms of carbon fiber strands after polymer burn off and deplying showing the multitude of shapes and sizes of strand fragments within the volume in Fig. 3(b). The unidirectional fiber strands can be locally represented in the volume as randomly oriented superposed layers as in Fig. 3c. The relatively limited fiber length and the random orientation of the strands within the volume make the Classic Lamination Theory (CLT) no longer directly applicable.

Fig. 3 (a) CF-SMC material volume; (b) the CF fiber strands of the volume after matrix elimination;(c) schematic representation of the material implementation in the model

2.1 Model description

Feraboli, [7], circumvented the problem and adapted an earlier model of Halpin and Pagano, [10], based on the assumption that, being the fiber orientation completely random, the material as a whole is characterized by a long distance disorder. On a local scale, however, the finite fiber length (from 8mm to 50mm) defines the material structure as an ordered one. This leads to two main consequences: i) the CLT can be used to describe the material behavior at a short distance scale; ii) the size of the domains where the CLT can be applied (defined as Randomly Representative Volume Elements, or RRVE) has to be defined. The mechanical behavior of the real material helps the identification of the size of the representative domains. The implementation of material model is focused on every single RRVE, where the reinforcement is defined in a random way, Fig. 3c. Specifically, every material layer is synthetized by randomly generating both the fiber orientation and the surface area of the layer itself. When the volume of material laid down reaches the target value occupied by the real RRVE, the volume of material with a certain in – plane orientation is calculated. Knowing the surface extension of the RRVE, a thickness value is then obtained for every material layer. The final local laminate is symmetric, while the stacking sequence is defined by randomly sorting out all the layers. Therefore, the final laminate is equivalent to the actual virtual SMC, generated platelet by platelet and it will have layers of different thickness, proportional to the amount of material with a certain fiber direction. A final discretization according to a specified number of in – plane fiber orientation is introduced.

For a better understanding of the original model configuration and implementation for tensile specimen, the [7] paper must be taken as a reference.

2.2 Model Implementation

The modelling approach of [9] was implemented and initially tested considering the simple geometry of tensile specimens. However, the aim of the present paper is its application to complex shell – like structures. Therefore, an efficient modeling approach involving the automatic generating all the model partitions was developed to expedite the task of defining hundreds of RRVEs as typical of large structures. Fig. 4 shows the work flow of the proposed implementation. It uses two commercial FE codes (Hyperworks and Abaqus) and an original two-part software developed in the Octave environment.

Quadrangular shell elements "QUADS" in Altair Hypermesh® are initially used to define a regular mesh. The file containing the mesh – related information (nodal coordinates, element-nodes connectivity), i.e. a text file, is processed with a specific software routine in order to organize elements groups ("SETs") representing the computational version of the RRVEs (in this way, the acronyms "SET" and "RRVE" will be used as interchangeably).

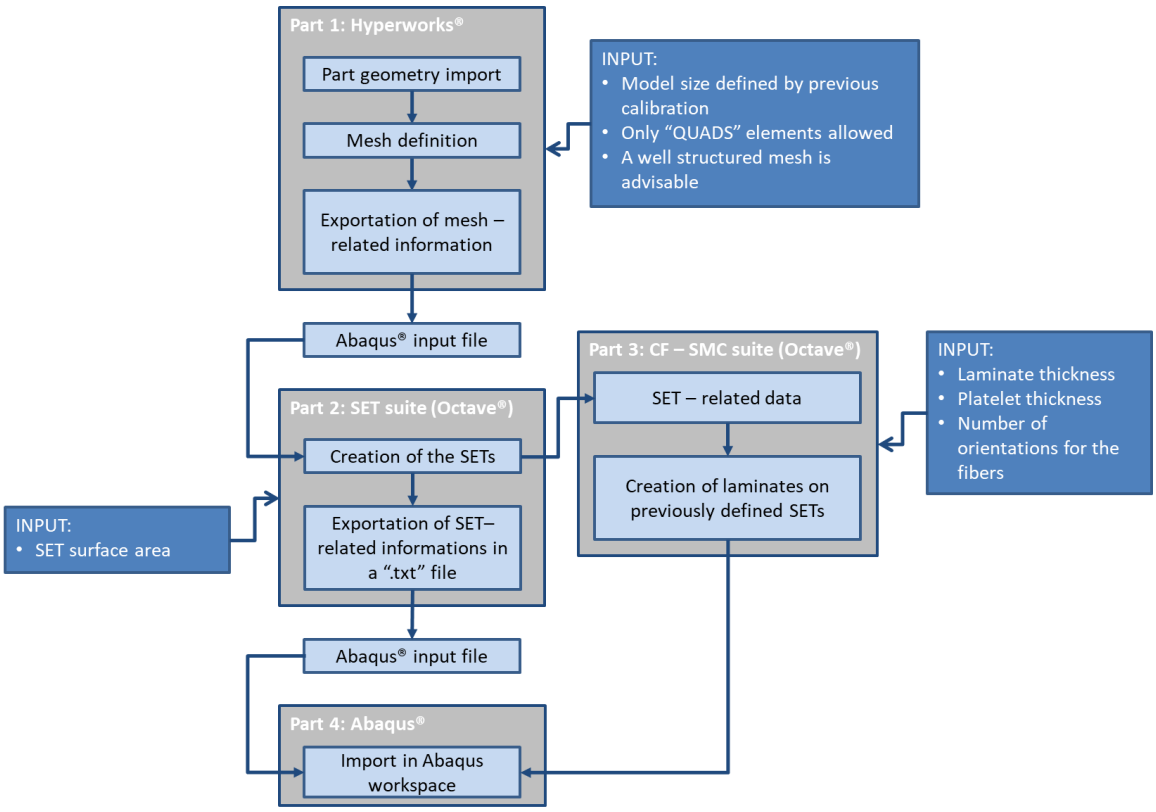

Fig. 4 Flow chart of the entire procedure for the model definition .

The material model is automatically laid down on the reference surface through random layer-by-layer generation of a single SET at a time (or RRVE). The random definition of the material is referred to both the surface area of every layer and its orientation. The approach adopted to group the elements in order to create the RRVEs previously defined is repeated multiple times through the entire mesh, recreating the same pattern. The number of elements for each group can be selected among i = 1, 2, 3 and 4, thus defining SET(i^2) as shown in Fig. 5. The routines used to define the SETs and to implement the material are written with Octave®.

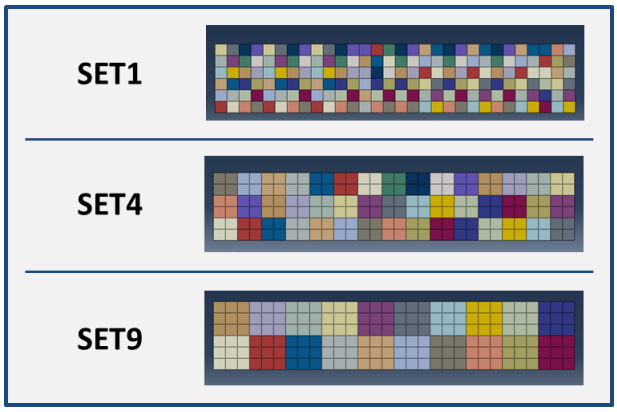

Fig. 5 Modeling of tensile specimens (38 x 200 mm2) with RRVE of different sizes

The starting mesh is the same for the three configurations, while RRVEs are identified by a monochromatic squared areas and feature an increasing level of structural detail. When the structured mesh is prepared and the material is implemented in the model, each partition can be imported in a FEA solver (here Abaqus ® by Simulia was used) and afterwards post processed for results.

3 Model calibration

Model calibration is achieved by exploration of the influence of different modeling parameters in the model predictions and by their identification using experimental results as reference. Here only results from tensile tests are considered for space limitations, although the present authors developed and used also flexural tests. Initially the experiments reported in [9] are used to calibrate the present software implementation. Then, original experiments from the authors' lab on a different and specific CF-SMC material processed by compression molding are used to calibrate the material response because used in the series production of the complex part to be investigated in the last section of this paper.

Elastic properties of the platelets used in [9] are shown in Tab.1. On the other hand, the properties of the present CF53%-SMC were not specified by the material producer so they were obtained by preliminary calibration with experiments and listed in Tab. 1.

Table 1: Elastic properties of the platelets dispersed inside the material

	E11 [MPa]	E22 [MPa]	G12 [MPa]	G13 [MPa]	G23 [MPa]
Feraboli [7]	113763	8412	4137	3759	3759
Present CF-SMC	78497	5804	2854	2594	2594

3.1 Virtual test setup and critical parameters

All experiments considered in this work followed the ASTM D 3039/D 3039M-00 standard, [11], specifically developed for tensile test on short fiber composite specimens. During the test, the load is applied to the specimen as a consequence of the translation of the moving head, which moves upwards at a constant speed, until the failure of the specimen. The Young's modulus is calculated as indicated by the next equation:

$$E = \frac{\sigma_2 - \sigma_1}{\varepsilon_2 - \varepsilon_1} = \frac{(\sigma(\varepsilon_2) - \sigma(\varepsilon_1))}{\varepsilon_2 - \varepsilon_1} \quad (1)$$

where ε_1=0.001mm/mm and ε_2=0.003mm/mm.

The correct size for the RRVE element is key for meaningful results. Its value is related to the size of the fiber domains. The peculiar meso – structure of a CF – SMC composite material has a strong influence on the mechanical behavior of the specimen. Specifically, the larger the size of these fiber domains (platelets) and the larger the scatter in the test results, both in terms of global mechanical strength and stiffness. A correct model implementation requires the correct ratio between the RRVE size and the overall specimen size.

This phase will be divided in two different steps: in the first one, an initial comparison will be developed between the DIC analysis results reported in [9] and the present model using the elastic properties of the platelets listed in the first row of Tab. 1. The subsequent series of numerical tests vs experiments using another CF-SMC material adopted the elastic properties also listed in Tab. 1 (second row).

3.2 Calibration using DIC analysis [7]

The tensile tests originally reported in [3] were characterized by the use of the DIC (digital image correlation) method in order to monitor the development of the superficial strain. In order to reproduce

the real tests, numerical DIC-like data are extracted during the post – processing phase, recording the local deformation of the virtual specimen for each node of the mesh. The aim is to reproduce the subset defined during the DIC analysis to recreate the surface strain pattern.

Two plots are shown in Fig. 6 where the present results in terms of longitudinal elastic modulus Ex of the virtual DIC analysis are compared with those obtained experimentally. The three models of Fig. 5 are kept as reference. Fig. 6a shows the "avgEx" parameter: this is the averaged value of the surface elastic modulus obtained with the DIC method. The value of this parameter is obtained by measuring the increasing local strain on the surface of the specimen in different instants of test; those values are then used to calculate the local elastic modulus, "Ex". A mean value is then calculated, "avgEx", which is the average superficial value for "Ex". Those calculations are then repeated for every (virtual or real) specimen involved, obtaining a value of "avgEx" for each one of them. Starting from those results, further parameters are also calculated: the mean value (avg(avgEx)) for "avgEx"; the minimum value (min(avgEx)) and the maximum value (max(avgEx)) for "avgEx". Those results are meant to be statistically representative of the overall behaviour of the (real or virtual) specimens. Fig. 6b shows the values of the coefficient of variation for "avg(Ex)".

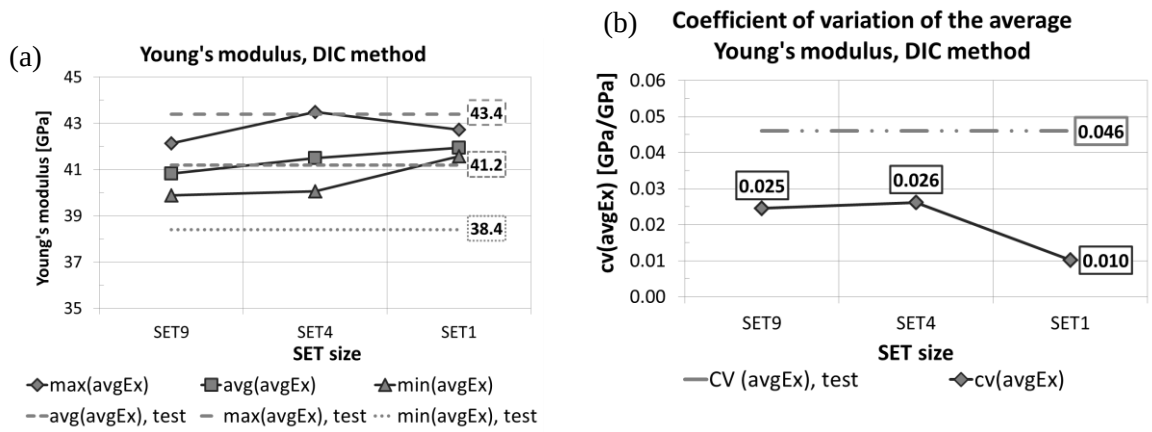

Fig. 6 Calibration tests based on the DIC analysis, [7];Mesh used are shown in Fig. 4 (a) maximum, minimum and average values of the surface elastic modulus; (b) coefficient of variation of the elastic modulus

Starting from the first graph, moving from left to right, the number of RRVEs used increases and the "avg(avgEx)" value increases as well. It is a clear trend highlighting its linear dependence of that parameter from the number of domains involved in the model definition. This behavior is related to an increasing structural redundancy of the material. In facts, the overall elastic properties of a virtual specimen directly rely on those of the local laminates. As the number of RRVEs increases, the dependence between local and overall elastic properties becomes weaker and weaker: the most compliant local laminates will be less effective in increasing the compliancy of the virtual specimen, resulting in generally stiffer specimens.

The other parameters "max(avgEx)" and "min(avgEx)" converge in the first graph towards avg(avgEx). This trend is confirmed by the second graph, in which CV(avgEx) from 0.025 to 0.010, switching from a SET4 configuration to a SET1 configuration. This effect is still related to the increased model redundancy, that brings the model to decrease the variability of the results.

The best set-up is the one indicated as "SET4" configuration because the average behavior of the generic virtual specimen is the closest to the experimental one. The model underestimates the actual variability of the behavior, possibly because the model hypothesis excludes out – of – plane fiber orientation and the presence of material internal flaws.

3.3 Calibration using ad-hoc tests

In this paragraph, results obtained with original tensile tests will be compared with those obtained with the present model. Two modelling configurations characterized by the same SET structure and two different sizes of the RRVEs are shown in Fig. 7(c). Every RRVE is represented by a monochromatic squared area. Fig. 7(a) and Fig. 7(b) show the influence of the number of in – plane fiber directions implemented on the elastic modulus. "Ex" is the generalized Young modulus calculated for every (virtual or real) specimen: it is so calculated as indicated in equation (1), where the strain is obtained through the overall elongation of the specimen. From those values, the maximum (max(Ex)), minimum (min(Ex)) and mean value (avg(Ex)) are then calculated (Fig. 7(a)). The coefficient of variation (CV(Ex)) is also calculated (Fig. 7(b)).

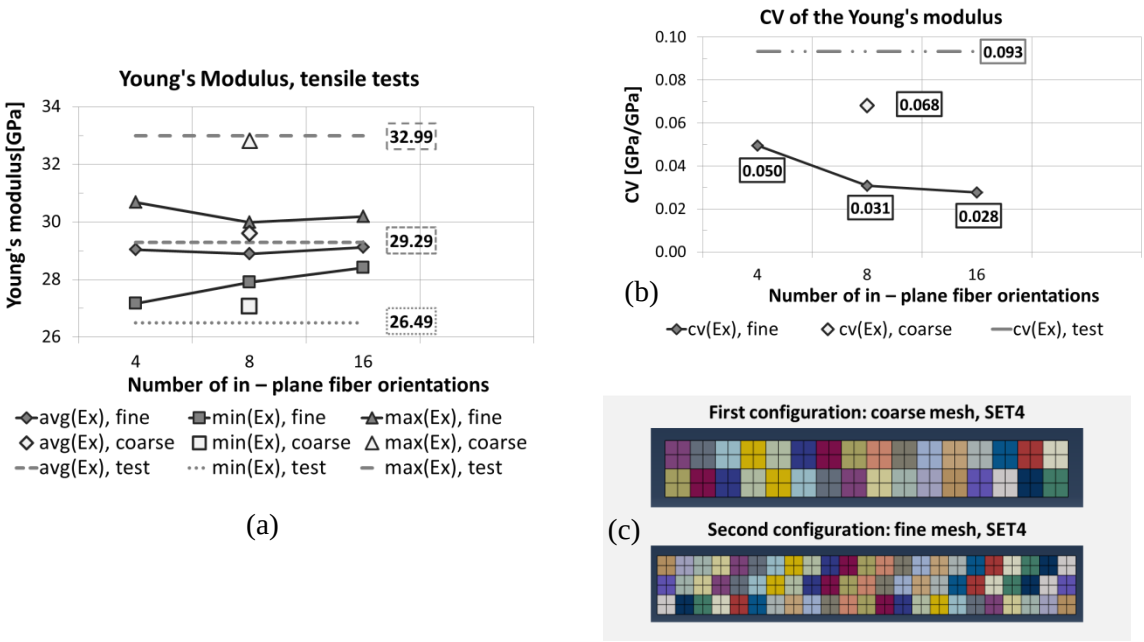

Fig. 7: Results of the calibration based on the tensile tests, []; (a) maximum, minimum and average values of the elastic modulus; (b) coefficient of variation of the elastic modulus; (c) mesh used to model specimens (15x140 mm2)

Focusing on the fine mesh curves (indicated with "fine"), Fig. 7a shows that the number of orientation directions doesn't affect the average value of the elastic modulus. At the same time, there's a clear convergence of max(Ex) and min(Ex)curves toward the avg(Ex) with increasing number of fiber directions. This behavior can be explained with a reduction of the structural redundancy of the virtual material for the elastic response. In facts, every layer of material is highly anisotropic: increasing the number of orientations increases the number of layers for every local laminate (there's a layer of material for every in – plane orientation): this brings to the reduction of the elastic anisotropy of the single RRVE, consequently decreasing the Young's modulus variability. This effect is quantified by CV(Ex) in Fig. 7(b).

Furthermore, a comparison between the two meshes ("fine" and "coarse") is provided for the 8 directions configuration. As shown by the first graph, the model with the coarser mesh provide a considerably wider range of values for the elastic modulus, confirming what was already observed in the previous paragraph: increasing the size of the RRVEs (so reducing the number of them) leads to a reduction of the elastic redundancy that produce a less predictable elastic behaviour. A further and more accurate comparison is certainly provided by the second graph, where the CV(Ex) parameter shows a remarkably higher value for the coarser mesh. The size of the elements adopted seems not to affect the performance of the model.

In conclusion, the coarse mesh, with 8 fiber in – plane directions implemented is finally proposed for the present CF SMC material as it provides the best fit to experimental results.

4 Modelling approach applied to component

After the model calibration phase using the simple tensile specimen geometry, now the structural modeling method for CF-SMC is applied to the real component shown in Fig. 8a. It is a section of the rear window frame of a sport car whose geometry is considerably more complex than the previous tensile specimen. This part was tested under three-point bending loading in the laboratory, Fig. 8b, on a servo-hydraulic MTS810 test machine. Bending tests were under displacement control condition and the load were monitored up to part failure.

Here the bending experiment is modeled using the FE implementation of the modeling approach described in the previous sections. The cylindrical surfaces of Fig. 8b represent the three rollers in contact with the part during the test. The roller/part contact was simplified in the FE analysis through equivalent line loads.

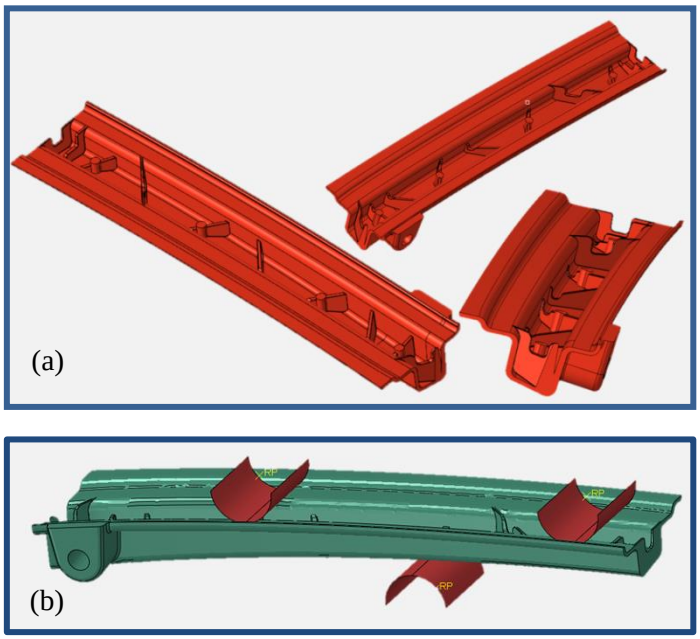

Fig. 8 (a) Geometry of the CF-SMC structural part (b) scheme showing the rollers applying a three point bending to the part.

The modeling method of the previous section is successfully applied to a simple geometry. When considering realistic 3D structures as that of Fig. 8 (a), a regular mesh may not be readily defined. In the approach used here, the geometry was partitioned and meshed regularly, where possible, with suitable SET definition. The irregular sections were also meshed, locally checked and their influence assumed negligible on the overall computed behavior. Other approaches aimed at overcoming this approximation are currently under development.

Fig. 9(a) and 9(b) show the modeled part with evidence of regular square SETs used for the rectangular regions. The previous calibration phase identified an ideal SET size of approx. 140mm^2. However, the theoretical SET shape and size enters in conflict locally with the actual part geometry (i.e. in the central ribbed part) leading to inhomogeneous element size and loss of structural order in the definition of the mesh with element distortion in critical areas. The prescribed SET definition is not applicable there and the software may not converge to the exact solution because of incomplete SETs. Since the size of the SETs / RRVEs controls the variability in the elastic performance of the

model, a fictitious effect is introduced. Fig. 9(c) shows the stress distribution at maximum bending load. The heterogeneous stress is due to the random description of each RRVE.

The comparison between experimental load – displacement curves and the elastic response of the present model is shown in Fig. 10. The experimental tends show a linear elastic behavior (after a small setting phase) followed by progressive damage up to failure or test interruption for excessive damage accumulation. The broken-line linear trends are obtained using the current model implementation applied to the part geometry after 5 different random material depositions. The correlation between experimental and simulated stiffness is quite good as described by the data of Table 2. The average elastic behavior is close to the average experimental response although the stiffness variability of the real part is larger than predictions.

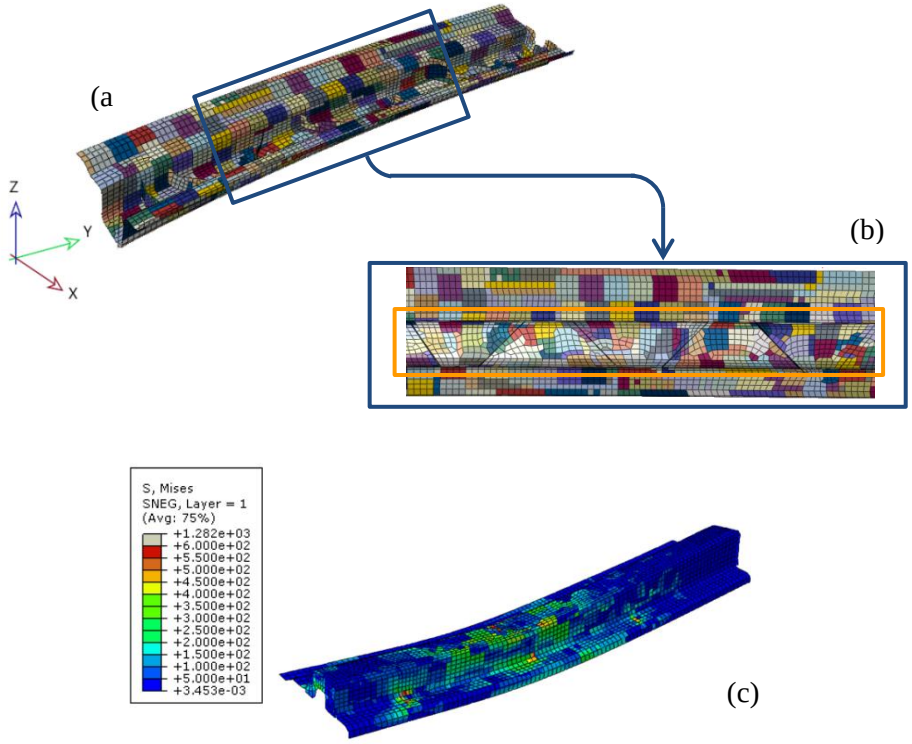

Fig. 9 a) FEA model of the part with evidence of SETs, b) focus on the ribbed region critical for regular SET definition c) Von Mises stress distribution under maximum bending load condition

The current level of development of the model is still limited. First, the onset and evolution of damage is not yet predictable. Second, there's not a clear connection between the shape of the real platelets and the one of the RRVEs used, while in literature it has been observed that in reality this aspect plays a fundamental role in defining the damage mechanics, both for initiation and grow.

From the CF-SMC modeling point of view, in addition to the limitations pointed out in the calibration section, the present model relies on the hypothesis that the fiber reinforcement is oriented in every possible in-plane direction with the same probability. Experimental evidence suggests that this is not true for a real part with complex geometry due to material displacement within the mold during compression molding. This may explain the reduced variability of the model performance in comparison with the real part. The presence of incomplete SETs due to geometrical complexity lead to an unwanted size reduction with a reduced influence on scatter of the elastic behavior.

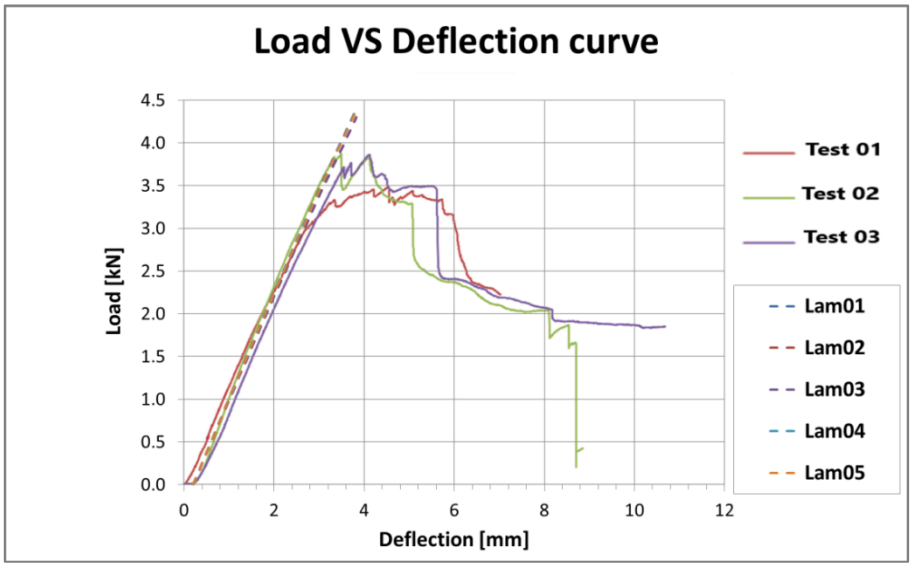

Fig. 10 Structural response of complex CF SMC part in bending: FE modeling vs experiments

Table 2 Elastic response of the CF-SMC structure under three point bending

Loading point deflection [mm]	Predicted stiffness [kN/mm]	Experimental stiffness [kN/mm]
0.0	$1.25^{+0.03}_{-0.02}$	
0.5	$1.25^{+0.03}_{-0.02}$	$1.29^{+0.14}_{-0.26}$
1.0	$1.24^{+0.03}_{-0.02}$	$1.29^{+0.20}_{-0.02}$
1.5	$1.22^{+0.03}_{-0.02}$	$1.23^{+0.06}_{-0.19}$
2.0	$1.20^{+0.02}_{-0.03}$	
2.5	$1.18^{+0.02}_{-0.03}$	

5 Conclusions

This contribution described the development of a structural modeling strategy for parts made of advanced CF-ROS composite processed by compression molding. The main conclusions reached are the following:

- the statistical model proposed in [9] for the CF-ROS material elastic response has been implemented within an efficient FEA-based part modeling work flow.

- The model implementation has been validated and the CF-SMC material calibrated by comparison of model predictions and experimental results of simple tensile tests both from the literature and from a specific test program.
- The integrated modeling procedure successfully predicted the average stiffness response of a compression molded part of complex geometry subjected to know loading conditions. However, the experimental scatter was considerably larger than predicted.

Acknowledgement

CPC Group (Modena, Italy) is gratefully acknowledged for providing the CF-SMC specimens and the automotive part that were tested for this work

References

[1] Knakal C, Wang C S, Dahl J S and Shah B 2011 Carbon Fiber SMC *Automotive Composites Consortium Technical Report*, ACC932-14

[2] Cabrera R M and Castro J M 2006 An economical way of using carbon fibers in sheet molding compound compression molding for automotive applications *Polym Compos* **27** 718–22.

[3] Feraboli P, Gasco F, Wade B, Maier S, Kwan R, Masini A, DeOto L, Reggiani M 2011 Lamborghini Forged Composite® Technology", ASC Technical Conference (Montreal: Canada)

[4] Van Wijngaarden M, Jongbloed A M and de Vries J 2010 Thermoplastic compound compression molding *Procs. International SAMPE Symp. & Exhib* (Seattle WA)

[5] https://www.roadandtrack.com/new-cars/car-technology/news/a32587/mclaren-brings-carbon-tub-production-home/ (retrieved 2020_08_10)

[6] Visweswaraiah S B, Selezneva M, Lessard L and Hubert P 2018 Mechanical characterisation and modelling of randomly oriented strand architecture and their hybrids – A general review *Journal of Reinforced Plastics and Composites*, **37**(8) 548–80

[7] Feraboli P, Peitso E, Deleo F and Cleveland T 2009 Characterization of prepreg-based discontinuous carbon fiber/epoxy systems *Journal of Reinforced Plastics and Composites* **28**, No. 10 1191-214

[8] Feraboli P, Peitso E, Cleveland T, and Stickler P B 2009 Modulus measurement for prepreg based discontinuous carbon fiber/epoxy systems *Jou. of Composite Materials* **43**, 1947-65

[9] Feraboli P, Cleveland T, Stickler P B and Halpin J C 2010 Stochastic laminate analogy for simulating the variability in modulus of discontinuous composite materials *Composites Part A Applied Science and Manufacturing* **41**(4), 557-70

[10] Halpin J C, Pagano N J 1969 The laminate approximation for randomly oriented short fiber composites *Polym Eng Sci*, 3 720.

[11] ASTM D3039 / D3039M-17, Standard Test Method for Tensile Properties of Polymer Matrix Composite Materials, ASTM International, West Conshohocken, PA, 2017